Journal of
Nanoscience and Nanotechnology
Vol. 6, 1–10, 2006

Oxidation–Reduction Dynamics in Layer-by-Layer Self-Assembled Redox Polyelectrolyte Multilayer Modified Electrodes

M. Tagliazucchi, D. Grumelli, C. Bonazzola, and E. J. Calvo

INQUIMAE, Departamento de Química Inorgánica, Analítica y Química Física,
Facultad de Ciencias Exactas y Naturales, Universidad de Buenos Aires, Argentina

The oxidation–reduction dynamics of layer-by-layer (LbL) self-assembled redox polyelectrolyte multilayer films on electrodes has been studied by cyclic voltammetry, chrono-amperometry, electrochemical quartz crystal microbalance (EQCM), ellipsometry, and Fourier transform reflection-absorption infrared spectroscopy (FT-IRRAS). Thin layer electrochemistry with fast electron transfer at the underlying metal-film interface and charge propagation by electron hopping between adjacent redox sites in the finite thin film has been observed. An almost ideal cyclic voltammetry for a fixed number of redox sites in the thin surface film suggests that the multilayer can be fully oxidized and reduced in the time scale of the experiment ($RT/vF \geq 0.05$ sec). The electron hopping diffusion coefficient 3×10^{-10} cm^2 s^{-1} was obtained from the chronoamperometric current transient and the ellipsometric thickness. Both cyclic voltammetry and potential step yield a surface osmium bipyridyl redox concentration of $\Gamma_{Os} = 4 \times 10^{-10}$ mol $\cdot$ cm^{-2} for (PAH-Os)$_5$(PVS)$_4$ film. Exchange of ions and solvent occur simultaneously to the charge injection as revealed by the EQCM mass change and the ellipsometric thickness change. From the end-to-end mass-to-charge linear relationship, the molar mass of the ionic and neutral species exchanged largely exceeds the molar mass of any ions or solvent which suggests an important flux of solvent during redox switching. An initial "break in" effect is observed for the first oxidation–reduction cycles when a newly self-assembled film equilibrates with the electrolyte as charge is injected during the electrochemical perturbation.

Keywords: Redox Polyelectrolyte, Layer by Layer, Osmium Bipyridyl, Ellipsometry, EQCM, Self-Assembled.

RESEARCH ARTICLE

1. INTRODUCTION

Decher et al. have introduced a method to prepare multilayered thin films by electrostatic interaction between oppositely charged polyelectrolytes.[1] In this method thin films comprised of charged polymers, proteins, DNA, etc. can be built up by sequential electrostatic adsorption layer-by-layer simply by alternate immersing a solid substrate in positive and negative polyelectrolyte solutions.[2, 3] A very large number of examples have been published with fine control of the film thickness with nanometer precision and control of surface charge.[4, 5] In particular, layer-by-layer self-assembled polyelectrolyte multilayers carrying redox active functionalities have been described in which charge can be switched in the redox centers by electrochemical reactions at the interface of the PEM's with the underlying electrode and charge transport in the film.[6, 7] Redox ions such as the anion $Fe(CN)_6^{4-}$ or the cation, $Os(bipy)_3^{3+}$ have been incor porated in these films from the electrolyte by ion exchange compensating charge. Thus the as formed intrinsic PEM incorporates redox charge by exchange of the polycation–polyanion ion-pair with redox anions in the electrolyte.[8] A number of redox polyelectrolyte multilayers (PEMs) with different redox groups attached covalently to the polymer back-bone such as viologen,[9–11] ferrocene,[12–19] osmium bipyridyl,[20–32] sulfonated polyaniline, polythiophene,[33] cytochrome c,[34] myoglobin,[35] polyoxo-metalates,[36] etc. have been reported. In LbL electrostatically self-assembled redox polyelectrolyte film modified electrodes the mass, thickness, and charge increase in each consecutive adsorption step.

Catalytic applications of multilayer films containing redox groups and enzymes have been reported in integrated supramolecular enzyme films.[12, 17, 20, 22, 27, 28, 37–40] In these systems a sequence of electron hopping events in the redox polymer is followed by electron transfer between some suitably positioned redox centers and the enzyme.

*Author to whom correspondence should be addressed.

The structure and dynamics of these self assembled redox active polyelectrolyte and enzyme multi-layers have been further investigated by quartz crystal microbalance (EQCM),[25] ellipsometry,[29–31] FTIR spectroscopy,[32] and Resonant Raman spectroscopy.[41] Nanoscale electrochemistry was realized in well organized self-assembled GOx-PAH-Os enzyme multilayers $(PAH\text{-}Os)_3(GOx)$ $(Apoenzyme\text{-}GOx)_3$, in which only one enzyme layer was active for the oxidation of β-D-glucose. Varying the relative position of the active enzyme layer in the nanostructure with alternating active and inactive FAD-free apoenzyme, we have shown that fast oxidation rates by a self-contained PAH-Os molecular wire can be achieved. The flux of electrons available is limited by the diffusion-like propagation of charge in the multilayer.[21]

A general feature of redox active multilayers on electrode surfaces is the exchange of ions and neutrals with the electrolyte during the oxidation and the reduction of redox polymer films to maintain electroneutrality in the film. Hillman et al.[42] reported the influence of swelling phenomena on mobile species transfer during redox switching of osmium bipyridyl polyvinylpyridine films prepared by droplet evaporation on electrodes. Anion or cation uptake or release from the film or a combination of both ion fluxes has been observed. However the fraction of redox charge compensated by either ion cannot be determined in electrochemical experiments alone since only the total charge exchanged with the electrolyte can be monitored.[43, 44]

Donnan permselectivity in layer-by-layer self-assembled redox poly-(allylamine) modified with osmium bipyridylpyridine complex (PAH-Os) and anionic poly(styrene) sulfonate (PSS) thin films has shown that the nature of the polyelectrolyte capping layer, the electrolyte pH, and the ionic strength determine the apparent redox potential of the Os redox couple.[26] LbL self-assembled redox PEM have the unique property of control of the surface charge which cannot be done in ramdom redox polymer hydrogels.

While anionic exchange is the main contribution to balance charge, probe beam deflection (PBD) studies have shown that the potential distribution at the self-assembled redox PEM/electrolyte interface determines the proportion of cation and anion exchanged in the oxidation and reduction of these films. Unlike ion exchange membranes, layer-by-layer (LbL) electrostatically self-assembled polyelectrolyte multilayers, are reluctant amphoteric exchangers[9, 10] due to intrinsic compensation of polyion–polyion interactions in the film. These result in excess of charge localized at the upper polymer/electrolyte interface compensated by mobile ions in the solution.[44] In redox active multilayers the charge of the constituent polyelectrolytes can be altered by oxidation–reduction of redox centers after film build up, this may result in changes in ion or salt population within the multilayer (*extrinsic* charge compensation).[9, 10] The present contribution describes the oxidation–reduction dynamics of layer-by-layer self-assembled redox polyelectrolyte multilayer films on electrodes using several complementary techniques: Cyclic voltammetry, chronoamperometry, electrochemical quartz crystal microbalance (EQCM), ellipsometry, and Fourier transform reflection-absorption infrared spectroscopy (FT-IRRAS). While previous reports are of qualitative nature, the present study presents a more quantitative analysis of the different experimental evidences.

2. EXPERIMENTAL DETAILS

2.1. Reagents and Materials

All reagents were used as supplied and solutions were prepared from Milli Q (Millipore) deionized water. The osmium bipyridine derivatized redox polymer $Os(Bpy)_2$ $ClPyCH_2NH$-poly(allylamine), (PAH-Os), was synthesized as previously reported.[45] Polymer solutions were dialyzed against water and used without further purification. Thiol solutions of 20 mM 3-mercapto-1-propane-sulfonic acid (MPS) (Aldrich) in 16 mM sulfuric acid (Merck), were prepared before each experiment in order to avoid oxidation in air.

2.2. Surface Modification

Gold coated silicon (100) substrates were employed as electrodes with a 20 nm titanium and 20 nm palladium adhesion layer and a 200 nm gold layer thermally evaporated on silicon with an Edwards Auto 306 vacuum coating system, at $P < 1.10^{-5}$ mbar.

In the first step, the freshly evaporated gold film substrates were primed with sulfonate groups by immersion in an MPS solution for 30 min followed by rinsing with deionized water. After thiol adsorption, the first polycation layer was deposited on thiol-modified Au substrate by immersion in PAH-Os solutions for 15 min. The next and subsequent layers were deposited onto the modified surface by alternate immersion in a solution of the respective polyanion (PVS) for 15 min and polycation (PAH-Os) solution, followed by thoroughly rinsing with Milli-Q water. The adsorption times were determined by ellipsometric transient measurements and EQCM.[12] LBL supramolecular structures comprised of PVS/PAH and PVS/PAH-Os were built up by reverting the surface charge of the topmost layer.

The next and subsequent layers were deposited onto the modified surface by alternated immersions in a PSS or PVS solution for 10 min and PAH-Os solution (pH = 8.3), respectively and were thoroughly rinsed in deionized water at the end of each adsorption step. As PAH-Os has primary amine groups, it is approximately 80% protonated at the solution pH. No desorption of GOx was observed with the quartz crystal microbalance during rinsing steps.

2.3. Electrochemical Experiments

A standard three-electrode electrochemical cell was employed with an operational amplifier potentiostat (Autolab., Ecochemie, Holland). For reference electrode, Ag/AgCl; 3 M KCl was employed and all electrode potentials herein are referred to it; a platinum gauze auxiliary electrode of large area was employed. All electrochemical experiments were carried out at room temperature (20 ± 2) °C.

2.4. Electrochemical Quartz Crystal Microbalance

The quartz crystal resonator at 10 MHz was used as a quartz crystal microbalance (QCM) with a complex voltage divider to measure the resonant frequency and both of the components of the quartz crystal Butterworth-Van Dyke equivalent circuit, which has been described elsewhere.[46] AT-cut 10 MHz quartz crystals (International Crystal Manufacturing Company Inc., Oklahoma City, (cat. no. 31210), 14-mm-diameter and 0.168-mm-thick with an active area of 0.196 cm^2) with a roughness factor of 1.2 measured by AFM were employed. The crystals were mounted in the cells by means of viton O-ring seals, with only one face in contact with the electrolyte; this electrode was a common ground to both the ac and dc circuits.

2.5. Ellipsometry

Ellipsometric Measurements were employed to determine the thickness of the self-assembled multilayer films, using a SENTECH (Berlin, Germany) variable angle rotating-analyzer automatic ellipsometer (vertical type, 2000 FT model) equipped with a 632 nm laser as polarized light source. All measurements were performed at an incidence angle of 70.00°. The gold electrode was horizontally mounted in a Teflon holder and aligned before each experiment. All adsorption steps were carried out avoiding any variations of the electrode position in order to keep the system alignment. Ellipsometric parameters variation lower than the data dispersion for a single measurement (0.01 in Ψ and 0.05 in Δ) was guaranteed in this way.

Ellipsometric angles Ψ and Δ were determined from reflection-induced changes in the state of polarization of linearly polarized light, which are related to the ellipsometric ratio:[31]

$$\rho = \tan(\Psi)\exp(\Delta \cdot i) = \frac{r_p}{r_s}$$

where tan Ψ represents the amplitude change in ρ, Δ is the phase difference change, and r_p and r_s are the complex reflection coefficients for light polarized parallel and perpendicular to the plane of incidence which depend on the structure and optical properties of the system. Ellipsometric parameters (Ψ and Δ) were collected in operator-triggered mode after each adsorption step with the modified electrode surface in contact with TRIS 20 mM–KNO_3 0.2 M pH 7.4 buffer solution in a SENTECH liquid cell (E-SE400-20) fitted with two glass optical windows positioned for 70.00° with an accuracy of 0.01°. The experimental data were fitted as described elsewhere.[24]

2.6. Fourier Transform Infrared Spectroscopy

Reflection absorption spectroscopy (IRRAS) mode was employed using a Nicolet 510P spectrometer fitted with a DTGS detector and a Balston 75-45 purge gas generator. Reflection-absorption spectra were obtained for gold films modified with LBL redox PEMS using a purpose built reflectance set up with at 80° angle of incidence and a bare gold surface as background (reference). All spectra were collected at 4 cm^{-1} spectral resolution using 100 scans and are presented without smoothing correction.

3. RESULTS AND DISCUSSION

The simplest approach to study the oxidation and reduction processes of redox species confined to a thin film at an electrode surface is to vary the electrode potential with a triangular wave perturbation and to record the resulting current-potential curves.

Figure 1A depicts a typical steady state cyclic voltammogram (after few repetitive oxidation reduction cycles) for a film comprised of $(PAH\text{-}Os)_4(PVS)_4(PAH\text{-}Os)$ in 0.2 M KNO_3 electrolyte solution of pH 7.4 (20 mM TRIS buffer solution) at a scan rate of 50 $mV \cdot s^{-1}$. Oxidation and reduction peaks are almost the specular image of each other centered at 0.30 V with 90 mV of width at half height (FWHH). The peak current at $E^{0'} = 0.30$ V has a linear dependence on the potential scan rate below 0.5 V s^{-1} which indicates that all redox sites in the thin film can be oxidized and reduced in the time scale of the experiment, ca. $RT/vF \geq 0.05$ sec. The surface wave shown in Figure 1A is almost ideal with the peak separation at 50 $mV \cdot s^{-1}$ of only 4 millivolts. For a thin film containing a fixed number of redox centers that can be fully oxidized or reduced in the time scale of the cyclic voltammetry experiment, and for the total surface osmium concentration that fulfils the condition: $\Gamma_{Os} = \Gamma_{Os(II)} + \Gamma_{Os(III)}$, the current is given by:

$$i = i_{dl} + \frac{F^2 v \Gamma_{Os}}{RT} \frac{\exp\left[\left(\frac{F}{RT}\right)(E - E^{0'})\right]}{\left[1 + \exp\left(\frac{F}{RT}\right)(E - E^{0'})\right]^2} \qquad (1)$$

where the double layer charging current is given by $i_{dl} = C_{dl}v$ with C_{dl} the electrode capacitance, v the electrode potential sweep rate, $(v = dE/dt)$, F the Faraday constant (95487 C), R the universal gas constant, T the absolute temperature, E the electrode potential with respect to a suitable reference and $E^{0'}$ the formal standard electrode potential.[47]

Equation (1) assumes fast electron transfer kinetics at the interface of the underlying metal and the LbL

RESEARCH ARTICLE

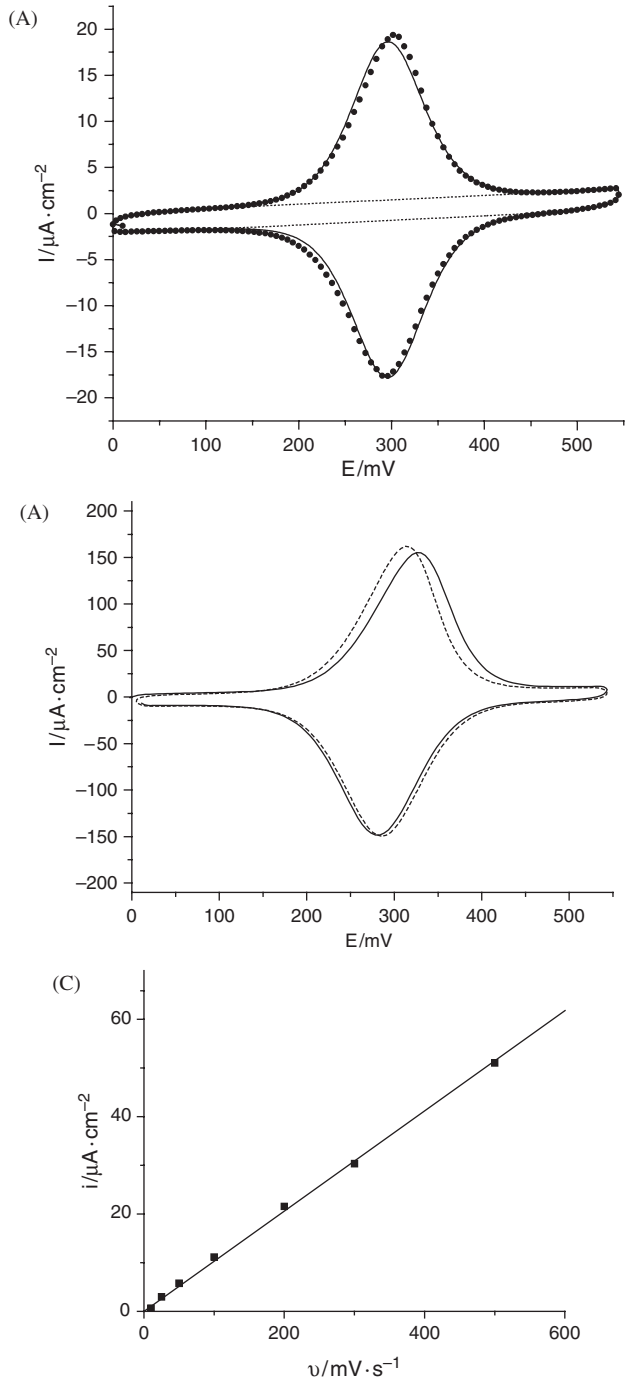

Fig. 1. (A) Cyclic voltammetry of $(PAH\text{-}Os)_4(PVS)_4(PAH\text{-}Os)$ in 0.2 M KNO_3, 20 mM TRIS buffer of pH 7.4 (points) and best fit to Eq. (1) (solid line) for $\Gamma_{Os} = (3.32 \pm 0.04) \cdot 10^{-10}$ mol · cm^{-2} (correlation factor 0.9989). (B) First cycle of a newly self-assembled electrode (solid line) and repetitive subsequent cycles (dotted line). (C) Plot of oxidation peak current versus sweep rate.

redox polyelectrolyte film with fast mass transport in the film as compared to the cyclic voltammetry characteristic time, RT/Fv. It also assumes an ideal behavior with no interactions between adjacent redox sites and a full width at half maximum of 90.6 mV at 25 °C. The cyclic voltammetry departs from this ideal behavior above 0.5 V s^{-1}. In Figure 1A we compare the experimental cyclic voltammetry data at low scan rate with the best fit to Eq. (1) for $\Gamma_{Os} = (3.7 \pm 0.1) \cdot 10^{-10}$ mol · cm^{-2} and $E^{0'} = 0.296$ V. Excellent agreement is found with an ideal full width at half maximum (FWHM) of 90.6 mV and a double layer capacitance of 10 μF cm^{-2} in good agreement with the value obtained from Electrochemical Impedance Spectroscopy (EIS), 7.5 μF cm^{-2} (Ref. [48]).

From Eq. (1) we can deduce that the peak current at $E = E^{0'}$ is given by:

$$i_{peak} = i_{dl} + \frac{F^2 v \Gamma_{Os}}{4RT} \quad (2)$$

which follows a linear dependence on the potential sweep rate as shown in Figure 1C. From the slope we obtain the electroactive surface concentration of osmium bipyridyl complexes in the film, $\Gamma_{Os} = (3.32 \pm 0.04) \cdot 10^{-10}$ mol · cm^{-2} (correlation factor 0.9989) in good agreement with direct integration of the surface wave for $v \leq 500$ mV s^{-1}.

Figure 1B shows a comparison of the first linear scan voltammetry for an electrode freshly prepared by LbL self-assembly and a stable voltammetry after the second and subsequent scans. At 0.5 V s^{-1} a more irreversible cyclic voltammogram is observed in both cases and the first oxidation–reduction cycle always shows larger anodic to cathodic peak separation due to the conditioning process known as "break in" by which the film after charge injection equilibrates with solvent and electrolyte.

The shape and position of cyclic voltammograms for this redox multilayer system strongly depends on the nature of charge in the topmost layer, the electrolyte pH and ionic strength. In the present communication for simplicity we show the most ideal case. Less reversible and more complex kinetics have been found for redox PEMs with negatively charged topmost layer at low ionic strength.[48] In that case, in addition to the charge transfer process at the Au-osmium film interface and electron hopping between adjacent redox centers there is a kinetic barrier. That kinetic hindrance may be related to the flow of anions at the film-electrolyte interface due to a skin Donnan barrier produced by the excess negative charge at the capping PVS layer[48] and is currently being investigated.

One limitation of cyclic voltammetry is that it is difficult to separate the effects due to the electrode potential from kinetics alone since the electrode potential is varied with time.

In a chronoamperometry, a complementary technique, a fast potential step is applied to perturb the redox concentration at the Au-film interface and the kinetics and mass transport at short times are obtained from the current-time relaxation. The advantage over cyclic voltammetry is the total separation of potential and time effects. Typical chronoamperometric current transients for full oxidation and full reduction of similar $(PAH\text{-}Os)_4(PVS)_4(PAH\text{-}Os)$

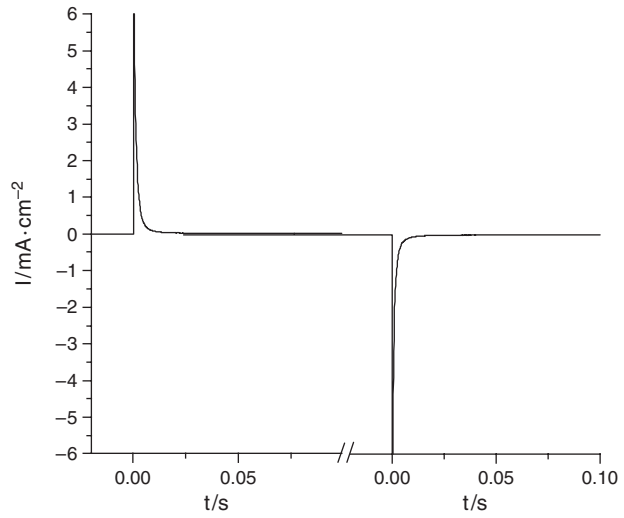

Fig. 2. Chronoamperommetry transients for the oxidation (A) and reduction (B) of osmium sites in $(PAH\text{-}Os)_4(PVS)_4(PAH\text{-}Os)$ in 0.2 M KNO_3, 20 mM TRIS buffer of pH 7.4 for a potential step from 0.10 V to 0.55 V.

films are shown in Figure 2. Integration of these current transients yields the amount of electrical charge involved in the electrochemical process.

Figure 3 depicts linear i versus $t^{-1/2}$ Cottrel plots[49] for depletion of the electroactive species near the electrode surface by semi-infinite diffusion within the film. Note however, that while this behaviour is closely followed at short times, a deviation is observed at longer times with lower currents than predicted by the linear current versus $t^{-1/2}$ relationship. Due to the finite thickness of the osmium film, a deviation below the current densities expected for semi-infinite diffusion both for the reduction and the oxidation branches is observed in Figure 3. As the Os(III) concentration profile inside the film spreads

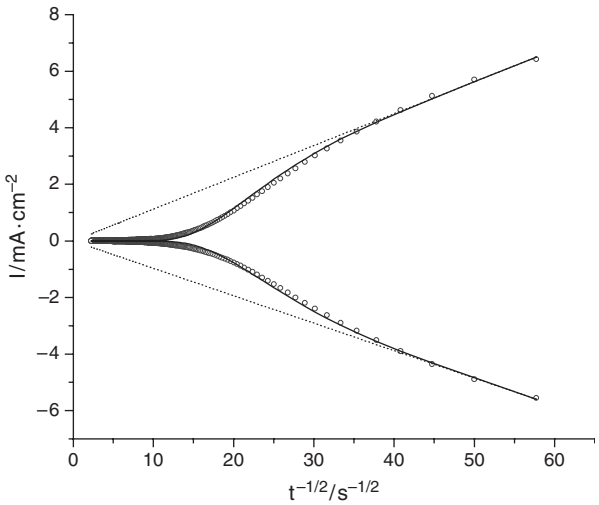

Fig. 3. Cottrell plot for the oxidation and reduction of osmium sites for the electrode in Figure 2. Solid lines: Best fit to Eq. (3). Dotted lines: Best fit to Eq. (5).

towards the film electrolyte interface, a change in boundary conditions at this interface forces a concentration gradient below the expected one for semi-infinite diffusion (see below).

The current transient for a bound diffusion within a finite thin layer containing redox species following a concentration step at the underlying metal-film interface is given by:[50]

$$i = \left(\frac{D}{l^2}\right)^{1/2} \Delta q (\pi \cdot t)^{-1/2} \left[1 + 2\sum_{m=1}^{\infty} (-1)^m \exp\left(-\frac{m^2 \cdot l^2}{D \cdot t}\right)\right] \tag{3}$$

where l is the film thickness, D the diffusion coefficient of the mobile species (electron hopping in the present case), Δq the total amount of charge injected into the film by the potential pulse. Notice that the important parameter in Eq. (3) is l^2/D, which results independent of electrode potential as expected for a pure diffusion process (i.e., negligible migration contribution to the electron transport).

Best fit of the experimental data in Figure 3 to Eq. (3) and the ellipsometry thickness $l = 10.3$ nm, yield the values of $D = 3.0 \times 10^{-10}$ cm^{-2} s^{-1}, $\Delta q = 11.8$ μC·cm^{-2} for the oxidation transients and $D = 3.6 \times 10^{-10}$ cm^{-2} s^{-1}, $\Delta q = 9.3$ μC·cm^{-2} for the reduction chrono-amperometric transient respectively. Ito and co-workers[19] reported similar Cottrell plots for ferrocene ultrathin multilayers but did not quantitatively describe the current-time relaxation.

The evolution of concentration profiles can be calculated from the best fit parameters to the experimental chronoamperometric transient and is given by the following expression:[51]

$$\frac{C_{Os(II)}(x,t)}{C_{Os_T}} = \frac{4}{\pi}\sum_{m=0}^{\infty}\frac{(-1)^m}{(2m+1)}\left[\exp\left(\frac{-D\pi^2 t(2m+1)^2}{4(l-x)^2}\right) \times \cos\left(\frac{(2m+1)\pi x}{2(l-x)}\right)\right] \tag{4}$$

Figure 4 shows the relative concentration profiles for Os(II) within the film and its time evolution after a potential step perturbation that depletes Os(II) instantaneously at the metal-film inner interface and propagates towards the film-electrolyte interface by electron-hopping diffusion in the film, with fast anion uptake from the electrolyte to compensate charge.

At shorter times, when the concentration profile produced by the electrochemical reaction develops within the film, i.e. $t \ll l^2/D$ then Eq. (3) can be simplified to the Cottrell equation:[47]

$$i(t) = \frac{FAD^{1/2}C^*}{\pi^{1/2}t^{1/2}} \tag{5}$$

where C^* is the concentration of the redox species in the bulk thin film. This behavior is observed in the linear portions of Figure 3 which extrapolate to zero as predicted by Eq. (5).

RESEARCH ARTICLE

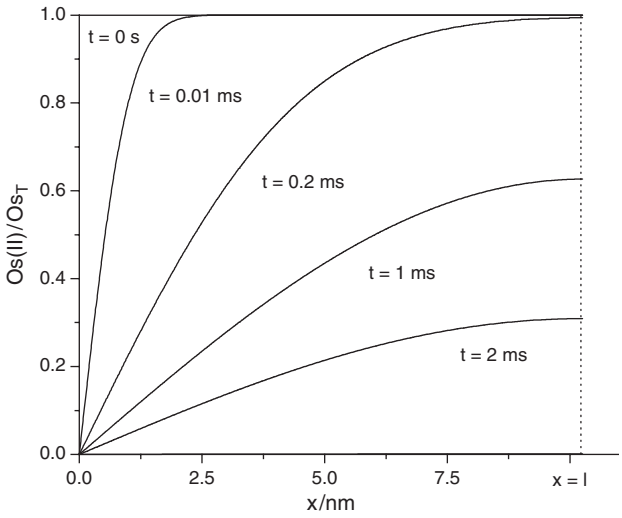

Fig. 4. Normalized Os(II) concentration profiles along the PEM film thickness at different times after the potential step from 0.1 V to 0.55 V for the oxidation of Os(II) calculated with Eq. (4) for $D = 3 \times 10^{-10}$ cm^2 s^{-1} and $d_f = 10.3$ nm.

It is worth considering the nature of the diffusion process in electrostatically self-assembled redox thin films in molecular terms. The osmium redox centers are covalently attached to the poly(allylamine) backbone, and they interact electrostatically with negatively charged PVS and mobile ions in the film. Therefore physical diffusion of redox centers can not contribute to the charge propagation.

Blauch and Saveant[52] introduced the concept of bounded diffusion to describe the physical displacement of the redox centers around their anchoring positions in the polymer backbone:

$$D_{\text{app}} = \frac{k_{\text{bim}}(\delta^2 + 3\lambda^2)C^*}{6} \tag{6}$$

where k_{bim} is the bimolecular activation-limited rate constant for electron hopping $k_{\text{bim}} = k_{\text{ex}}k_{\text{D}}/(k_{\text{ex}} + k_{\text{D}})$, k_{D} is the diffusion limited bimolecular rate constant and δ is the distance between adjacent redox centers in the film while λ represents the mean displacement of a redox center out of its equilibrium position. It can be related to an imaginary spring $\lambda = (2k_BT/f_{\text{s}})^{1/2}$, where k_B is the Boltzmann constant, T the temperature, and f_{s} is the spring force constant. Bourdillon and co-workers have recently presented an elastic-bounded diffusion model to describe the transient dynamics of a single layer of poly(ethylene glycol) chains bearing a ferrocene molecule (PEG-Fc).[53] An interesting concept introduced in this model is that as a consequence of the harmonic oscillations of the polymer chains, the concentration of redox sites in the self-assembled film follows a Gaussian distribution around the average anchoring plane:

$$C_{\text{Os}} = \frac{\Gamma_{\text{Os}}}{\sqrt{\pi}}\sqrt{\frac{f_{\text{s}}}{2RT}}\exp\left(-\frac{f_{\text{s}}x^2}{2RT}\right) \tag{7}$$

where x is the distance from the anchoring plane.

The spatial confinement of redox molecules within ultrathin films in well organized layers results in a "concentration anisotropy," which introduces new boundary conditions with an important entropic contribution. It is worth mentioning a recent report by Mao, Mano, and Heller of tris-dialkylated N,N'-bi-imidazole $Os^{III/II}$ polymer with a 13-atom spacer which shows an unprecedented large $D_e \approx 5.8 \times 10^{-6}$ cm$^2 \cdot$ s^{-1} (Ref. [54]). Ito and co-workers[19] have demonstrated the contribution of local segmental motions to the apparent diffusion coefficient of electron hopping charge propagation of self-assembled ferrocene modified polyacrylic-poly(2-methacryloyloxy)ethyl trimethyl ammonium chloride.

Since in our redox polymer the osmium bipiridyl center is attached to the PAH backbone by a 3 atom spacer, the value reported in this work for D_e is considerably smaller than that reported by Mao et al. However, it is in agreement with the value for $D_e \approx 1.9 \times 10^{-9}$ cm$^2 \cdot$ s^{-1} obtained for lateral diffusion in $[Os(bpy)_2(PVP)_2Cl]$[55] and with the value $D_e \approx 0.7 \times 10^{-10}$ cm$^2 \cdot$ s^{-1} obtained for Nafion films modified with $Os(bpy)_3^{2+}$ (Ref. [56]). It is important to mention that these are only qualitative comparisons since these osmium polymers have different redox concentration, i.e. see in Eq. (6) how the redox concentration influences on the apparent diffusion coefficient.

Electrochemical techniques such as cyclic voltammetry or chronoamperometry can only account for the exchange of electrons in the external circuit, while complementary techniques like the quartz crystal microbalance are able to measure the changes in mass and volume or viscoelastic changes due to the exchange of water and ions and their mechanical effects on the film properties.

The electrochemical quartz crystal microbalance (EQCM) has been used to measure the change in mass simultaneous to the chronoamperometric oxidation of $(PAH\text{-}Os)_{14}(PSS)_{14}PAH\text{-}OH$ films in 0.01 M NaCl solution for a potential step form 0.10 V in the Os(II) fully reduced state to 0.60 V in the Os(III) fully oxidized state. Figure 5A depicts gravimetry for a train of repetitive potential pulses applied to a freshly prepared $(PAH\text{-}Os)_{15}(PSS)_{14}$ film for the first few redox switching cycles.

An increase in the mass is observed in every oxidation step and a mass decrease in the subsequent reduction step to yield Os(II) film. However, the original mass of the fully reduced film is not recovered and a continuous mass increase in the film is apparent during several short oxidation–reduction cycles as seen in Figure 5A. Thus, a fraction of the species that get into the film from the electrolyte solution during oxidation, remains in the film in the following reduction cycle. Full recovery of the original mass is only observed if the electrode potential is kept constant at 0.1 V to a rest in the fully reduced state for more than one hour as shown in the transient of Figure 5B.

Comparison of the change in mass per unit area to the change in charge density during the end-to-end oxidation–reduction process results in a linear plot shown in

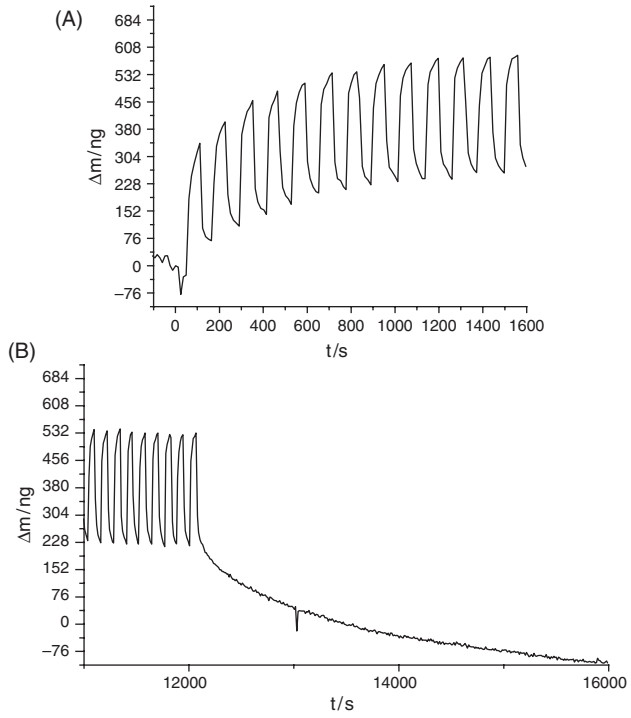

Fig. 5. EQCM gravimetric response of $(PAH\text{-}Os)_{15}(PSS)_{14}$ film in 10 mM NaCl for repetitive potential steps from 0.1 to 0. 6 V. (A) First switching cycles. (B) Electrode mass transient after switching off to 0.10 V.

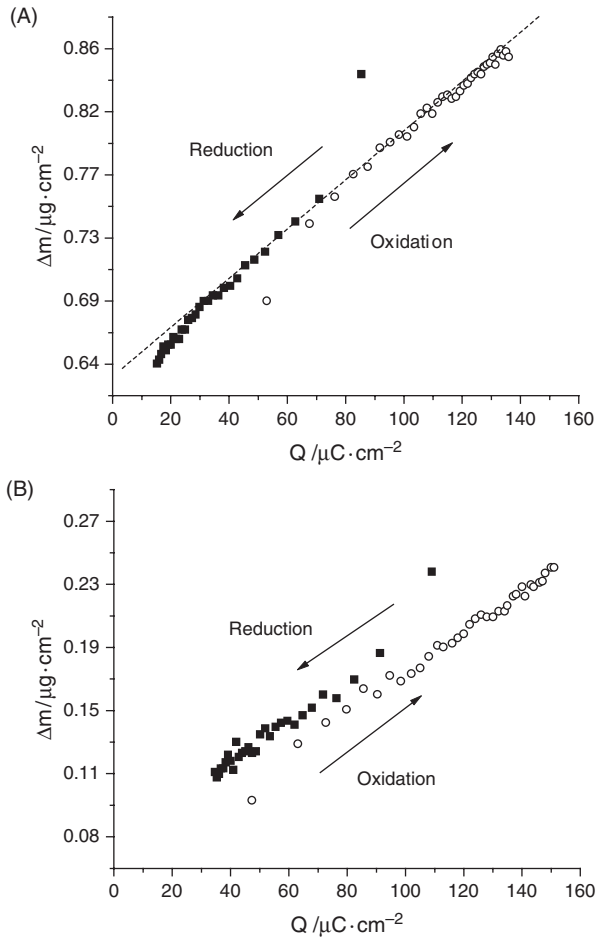

Fig. 6. End-to-end mass change to charge for the oxidation (open circles) and reduction (black squares) of osmium bipyridyl redox centers in $(PAH\text{-}Os)_{15}(PSS)_{14}$ films. (A) Steady state (cycle 32nd) and (B) first oxidation–reduction cycle. Open circles: Oxidation, black squares.

Figure 6. The EQCM measures the total mass of ions and neutrals (solvent and salt) exchanged at the film-electrolyte interface simultaneous to the injection of charge at the electrode-film interface in the potentiostatic step. From the slope in Figure 6A we have obtained a molar mass of 184 $g\,mol^{-1}$ in large excess with respect to the molar mass of the sodium (23 $g\,mol^{-1}$) and chloride ions (35.5 $g\,mol^{-1}$), respectively. Thus, we conclude that an important amount of neutrals are exchanged in the redox process. The study of different cations in the electrolyte has shown that this is a common behavior in these redox polyelectrolyte multi-layer films.[57]

The effect of the first oxidation step is seen in Figure 6B where some hysteresis is observed in the end-to-end mass to charge plot, and the reduction step of the first oxidation cycle shows a larger mass than the oxidation cycle. This should be related to the more irreversible cyclic voltammetry during "break in" for the first oxidation cycle shown in Figure 1C.

During oxidation and reduction of redox polymer films, exchange of ions with the electrolyte occurs to maintain the electroneutrality in the film. Anion or cation uptake or release from the film or a combination of both ion fluxes is possible. The study of Donnan permselectivity in layer-by-layer self-assembled redox poly(allylamine) modified with osmium bipyridyl-pyridine complex (PAH-Os) and anionic poly(styrene) sulfonate (PSS) thin films has shown that the nature of the polyelectrolyte capping layer, the electrolyte pH, and ionic strength determine the apparent redox potential of the Os redox couple.[26]

Radiotracer studies in poly(viologen)/poly(styrenesul fonate), (PSS), multi-layers revealled the exchange of both anion and cation.[10]

While anionic exchange is the main contribution to charge balance, preliminary reports by probe beam deflection (PBD) have shown that the potential distribution at the self-assembled redox PEM/electrolyte interface determines the proportion of cation and anion exchange during the oxidation and reduction of these redox active thin films.[58] In this technique a laser beam parallel to the electrode surface is deflected by the refractive index gradient that results from the ionic concentration gradient build up during the dynamics of ion exchange and reports the direction of the ion flux.

Changes in volume during redox switching have been studied with ellipsometry. During the oxidation of Os(II) films the thickness increases from 81 to 86 nm and the refractive index decreases from 1.515 to 1.495 as shown in Figure 7 for repetitive oxidation–reduction steps.

RESEARCH ARTICLE

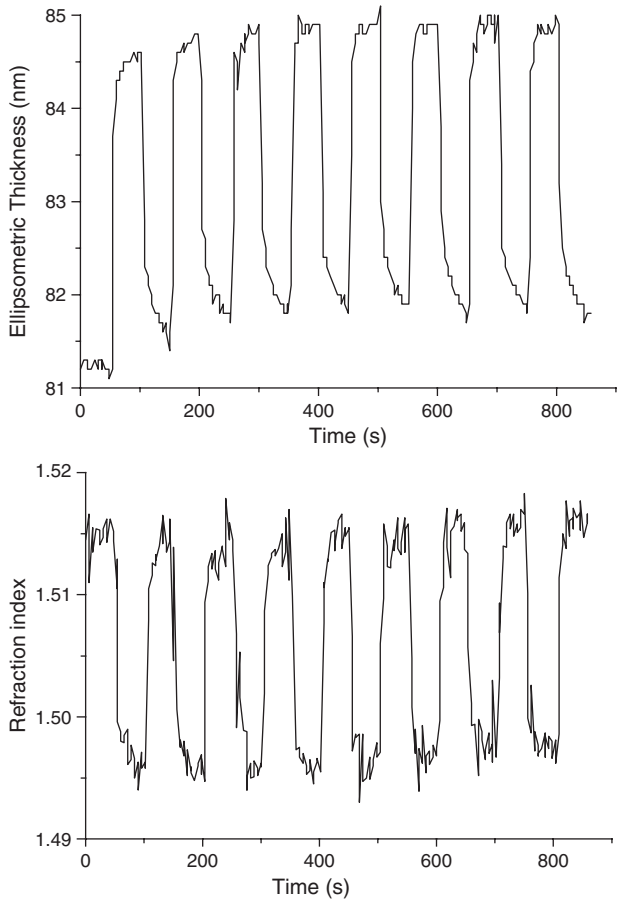

Fig. 7. Ellipsometric thickness and refractive index change for repetitive oxidation–reduction steps between 0.10 and 0.55 V for $(PAH\text{-}Os)_{15}(PSS)_{14}$ films in the conditions of Figure 5.

The swelling of the film is a consequence of the uptake of solvent in the oxidized state which also results in a slightly lower refractive index since the proportion of water ($n_{water} = 1.33$) increases with the degree of film oxidation.[29] Previous studies have shown that the amount of water exchanged with the electrolyte per mole of redox charge is constant, since a Nernstian dependence of the film thickness with the electrode potential is observed:[29]

$$d_f = d_f(\mathrm{Os(II)}) + \Delta d_f \frac{\exp\left[\left(\frac{F}{RT}\right)(E - E^{0'})\right]}{\left[1 + \exp\left[\left(\frac{F}{RT}\right)(E - E^{0'})\right]\right]^2} \quad (8)$$

A careful examination of Figure 7 for a repetitive potential square wave perturbation between oxidized and reduced states also shows that some equilibration phenomena occurs in the first few cycles with an increase in thickness that is not fully recovered upon reduction. Notice that while the refractive index oscillates between two average values, a continuous increase in film thickness is observed during the first few cycles until the film equilibrates as has been seen for mass increase with the quartz crystal resonator.

The parameters obtained in this work for the oxidation and reduction of PAH-Os redox PEMs are summarized in Table I. The ingress of neutral species during oxidation is supported from both the change in electrode mass and film volume. The lower refractive index of the oxidazed film suggests a higher water content in the oxidised films compared with the reduced form.

Table I. Characteristic parameters obtained for the electrochemical redox switching of LbL self-assembled PAH-Os/PVS multilayer films.

Osmium coverage (per PAH-Os layer)	7.0×10^{-11} mol · cm^{-2}
Electron hopping diffusion coefficient	$(3.3 \pm 0.3) \times 10^{-10}$ cm^{-2} s^{-1}
Exchanged mass (oxidation)[a]	184 g · mol^{-1}
Change in volume (oxidation)[a]	303 cm^3 · mol^{-1}
Refractive index of oxidized film[a]	1.515
Refractive index of reduced film[a]	1.495

[a]for a $(PAH\text{-}Os)_{15}$ $(PSS)_{14}$ film in 10 mM NaCl.

We can summarize the ion exchange that results from redox switching the polyelectrolyte multilayers for a 1:1 electrolyte, C^+A^- as follows: The following reactions are expected to occur during "break in" of a freshly prepared intrinsically compensated charge PEM:

$$[\mathrm{PAH\text{-}Os(II)}^+\,\mathrm{PVS}^-]_{poly} + A^-_{aq} + n\mathrm{H_2O} \rightarrow [\mathrm{PAH\text{-}Os(III)}^{2+}\,\mathrm{PVS}^-\,A^-\,n\mathrm{H_2O}]_{poly} + e(\mathrm{Au}) \quad (9)$$

$$[\mathrm{PAH\text{-}Os(III)}^{2+}\,\mathrm{PVS}^-\,A^-\,n\mathrm{H_2O}]_{poly} + C^+_{aq} + e(\mathrm{Au}) \rightarrow [\mathrm{PAH\text{-}Os(II)}^+\,\mathrm{PVS}^-\,A^-\,C^+(n-m)\mathrm{H_2O}]_{poly} + m\mathrm{H_2O} \quad (10)$$

for the oxidation and reduction respectively.

Once steady state has been attained for the hydrated extrinsic redox PEM with salt in the polymer multilayer, the following reactions should be considered:

$$[\mathrm{PAH\text{-}Os(II)}^+\,\mathrm{PVS}^-\,A^-\,C^+]_{poly} + xA^-_{aq} \rightarrow (1-x)[\mathrm{PAH\text{-}Os(III)}^{+2}\,\mathrm{PVS}^-\,A^-]_{poly} + (1-x)C^+_{aq} + x[\mathrm{PAH\text{-}Os(III)}^{+2}\,\mathrm{PVS}^-\,C^+\,2A^-]_{poly} + e(\mathrm{Au}) \quad (11)$$

Proof that water swells the film in every oxidation–reduction cycle and accumulates in successive oxidation–reduction cycles has been obtained from infrared reflection-absorption spectroscopy (FT-IRRAS) for $(PAH\text{-}Os(II))_{15}(PSS)_{15}$ in contact with the solution and under potential control. Figure 8 depicts the spectra for the 1648 cm^{-1} H_2O bending vibration for repetitive oxidation–reduction cycles. The numbers indicate the oxidation–reduction cycle number and the absorption spectra are substracted from the spectrum for the starting reduced film. The absorbance increases continuously with the number of oxidation–reduction steps, even though the spectra shown correspond to the reduced film. This evidence is consistent with the similar mass accumulation observed in Figure 5A for the EQCM gravimetric transient and increase in film thickness (Fig. 7).

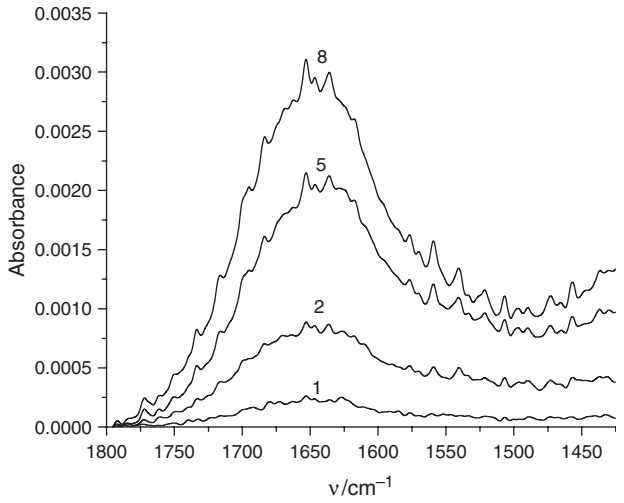

Fig. 8. FT-IRRA spectra for the H_2O band 1648 cm^{-1} (PAH-$Os(II))_{15}(PSS)_{15}$. Numbers indicate the oxidation–reduction cycle number.

In EQCM and ellipsometry faster transients are observed for the oxidation step than for the reduction. It is suggested that slow solvent relaxation in the film and exchange with the electrolyte during the reduction step accounts for this difference.

4. CONCLUSIONS

The construction of electrostatically self-assembled redox polymer and spatially organized multilayers allows to analyze the redox charge injection and transport along nano meter distances.

With such layer-by-layer self-assembled osmium bipyridyl pyridine complex modified poly(allylamine)-poly(vinylsulfonate) systems we have shown that oxidation occurs by fast electron transfer reaction at the underlying Au-film interface with further diffusion by electron hopping between adjacent osmium sites in the film. Cyclic voltammetry below 500 mV s^{-1} is slow with respect to the electron transfer reaction at Au so that the full oxidation–reduction of osmium spread throughout the entire film. Chronoamperometry in the millisecond range reveals the bound diffusion in the thin film while electrochemical quartz crystal microbalance (EQCM) and ellipsometry account for the change in mass and volume of the redox polyelectrolyte film due to the exchange of ions and solvent to equilibrate the ion population in the film after the injection of charge by electrochemical reaction. Fourier transform reflection-absorption infrared spectroscopy (FT-IRRAS) produces molecular evidence of water accumulation in the film in a time scale shorter than that needed to equilibrate the film with the electrolyte.

References and Notes

1. G. Decher and J. H. Song, *Phys. Chem.* 95, 1430 **(1991)**.
2. Y. Lvov, G. Decher, and G. Sukhorukov, *Macromolecules* 26, 5396 **(1993)**.
3. Y. Lvov, K. Ariga, I. Ichinose, and T. Kunitake, *J. Am. Chem. Soc.* 117, 6117 **(1995)**.
4. G. Decher, *Science* 277, 1232 **(1997)**.
5. G. Decher and J. B. Schlenoff, in *Thin Films—Sequentially Assembly of Nanocomposite Materials*, edited by G. Decher and J. B. Schlenoff, Wiley-VCH, Weinheim **(2002)**, Vol.
6. X. Zhang, J. Sun, and J. Shen, in *Multilayer Thin Films*, edited by J. B. S. G. Decher, Wiley-VCH, Weinheim **(2002)**, Vol.
7. B. Tieke, M. Pyrasch, and A. Toutianoush, in *Multilayer Thin Films*, edited by J. B. S. G. Decher, Wiley-VCH, Weinheim **(2002)**, Vol.
8. S. Han and B. Lindholm-Sethson, *Electrochimica Acta* 45, 845 **(1999)**.
9. T. R. Farhat and J. B. Schlenoff, *Langmuir* 17, 1184 **(2001)**.
10. T. R. Farhat and J. B. Schlenoff, *J. Am. Chem. Soc.* 125, 4627 **(2003)**.
11. J. Stepp and J. B. Schlenoff, *J. Electrochem. Soc.* L155 **(1997)**.
12. J. Hodak, J. R. Etchenique, K. Singhal, P. N. Bartlett, and E. J. Calvo, *Langmuir* 13, 2708 **(1997)**.
13. S. F. Hou, H. QA, and Y. Fang, *Chem. Anal. Lett.* 30, 1631 **(1997)**.
14. A. Liu and J. Anzai, *Langmuir* 19, 4043 **(2003)**.
15. V. Rosca and I. C. Popescu, *Electrochem. Commun.* 4, 904 **(2002)**.
16. A. Liu, Y. Kashiwagi, and J. Anzai, *Electroanalysis* 15, 1139 **(2003)**.
17. H. C. Yoon and H. S. Kim, *Anal. Chem.* 72, 922 **(2000)**.
18. H. C. Yoon, M. Y. Hong, and H. S. Kim, *Anal. Chem.* 72, 4420 **(2000)**.
19. T. Fushimi, A. Oda, H. Ohkita, and S. Ito, *Thin Solid Films* 484, 318 **(2005)**.
20. E. Calvo, F. Battaglini, C. Danilowicz, A. Wolosiuk, and M. Otero, *Faraday Discussion* 116, 47 **(2000)**.
21. E. J. Calvo, C. Danilowicz, and A. Wolosiuk, *J. Am. Chem. Soc.* 124, 2452 **(2002)**.
22. E. Calvo, R. Etchenique, L. Pietrasanta, and A. Wolosiuk, *Anal. Chem.* 73, 1161 **(2001)**.
23. E. J. Calvo, C. Danilowicz, and A. Wolosiuk, *J. Am. Chem. Soc.* 124, 2452 **(2002)**.
24. E. J. Calvo, E. S. Forzani, and M. Otero, *J. Electroanal. Chem.* 231, 538 **(2002)**.
25. E. J. Calvo, E. S. Forzani, and M. Otero, *Anal. Chem.* 74, 3281 **(2002)**.
26. E. J. Calvo and A. Wolosiuk, *J. Am. Chem. Soc.* 124, 8490 **(2002)**.
27. E. J. Calvo and A. Wolosiuk, *Chem. Phys. Chem.* 5, 235 **(2004)**.
28. E. J. Calvo and A. Wolosiuk, *Chem. Phys. Chem.* 43 **(2005)**.
29. E. S. Forzani, M. A. Perez, M. Lopez Teijelo, and E. J. Calvo, *Langmuir* 18, 9867 **(2002)**.
30. E. S. Forzani, M. A. Perez, M. L. Teijelo, and E. J. Calvo, *Langmuir* 18, 4020 **(2002)**.
31. E. S. Forzani, M. A. Perez, M. L. Teijelo, and E. J. Calvo, *Langmuir* 18, 9867 **(2003)**.
32. C. Bonazzola, E. J. Calvo, and F. Nart, *Langmuir* 19, 5279 **(2003)**.
33. J. Lukkari, M. Salomeki, A. Vinikanoja, T. Caritalo, J. Päukkunen, N. Kochanova, and J. Kankare, *J. Am. Chem. Soc.* 123, 6083 **(2001)**.
34. M. K. Beissenhirz, F. W. Scheller, W. F. M. Stöcklein, D. G. Kurth, H. Möhwald, and F. Lisdat, *Angew. Chem. Int. Ed.* 43, 4357 **(2004)**.
35. J. F. Rusling, in edited by Y. Lvov and H. Mowahl, Marcel Dekker **(2000)**, Vol.
36. L. Cheng, L. Niu, J. Gong, and S. Dong, *Chem. Mater.* 11, 1465 **(1999)**.
37. A. Narvaez, G. Surez, I. Catalin, C. Popescu, I. Katakis, and E. Domínguez, *Biosens. Bioelectron.* 15, 43 **(2000)**.
38. Y. Sun, J. Sun, X. Zhang, C. Sun, Y. Wang, and J. Shen, *Thin Solid Films* 730 **(1998)**.
39. C. Danilowicz and J. Manrique, *Electrochem. Commun.* 1, 22 **(1999)**.
40. W. Li, Z. Wang, C. Sun, M. Xian, and M. Zhao, *Anal. Chim. Acta* 418, 225 **(2000)**.
41. N. Tognalli, A. Fainstein, C. Bonazzola, and E. Calvo, *J. Chem. Phys.* 120, 1905 **(2004)**.
42. D. M. Kelly, J. G. Vos, and A. R. Hillman, *J. Chem. Soc. Faraday Trans.* 92, 4121 **(1996)**.

43. J. B. Schlenoff, H. Ly, and M. Li, *J. Am. Chem. Soc.* 120, 7626 **(1998)**.
44. J. B. Schlenoff and S. T. Dubas, *Macromolecules* 34, 592 **(2001)**.
45. C. Danilowicz, E. Corton, and F. Battaglini, *J. Electroanal. Chem.* 445, 89 **(1998)**.
46. E. J. Calvo, C. Danilowicz, and R. Etchenique, *J. Chem. Soc. Faraday Trans.* 91, 4083 **(1995)**.
47. A. J. Bard and L. R. Faulkner, in *Electrochemical Methods. Fundamentals and Applications*, edited by A. J. Bard and L. R. Faulkner, John Wiley, Inc., New York **(2001)**, Vol.
48. M. Tagliazucchi and E. J. Calvo, *J. Electroanal. Chem.* **(2005)**, submitted.
49. F. G. Cottrell, *Z. Physik. Chem.* 42, 385 **(1902)**.
50. W. J. Albery, M. G. Boutelle, P. J. Colby, and A. R. Hillman, *J. Electroanal. Chem.* 133, 135 **(1982)**.
51. D. M. Oglesby, S. H. Omang, and C. N. Reilley, *Anal. Chem.* 37, 1312 **(1965)**.
52. D. N. Blaunch and J. M. Saveant, *J. Am. Chem. Soc.* 3323 **(1992)**.
53. A. Anne, C. Demaille, and J. Moiroux, *J. Am. Chem. Soc.* 121, 10379 **(1999)**.
54. F. Mao, N. Mano, and A. Heller, *J. Am. Chem. Soc.* 125, 4951 **(2003)**.
55. A. P. O'Mullane, J. V. Macpherson, P. R. Unwin, J. Cervera-Montesinos, J. A. Manzanares, F. Frehill, and J. G. Vos, *J. Phys. Chem. B* 108, 7219 **(2004)**.
56. H. S. White, J. Leddy, and A. J. Bard, *J. Am. Chem. Soc.* 104, 4811 **(1982)**.
57. D. E. Grumelli, E. Forzani, C. Bonazzola, and E. J. Calvo, *J. Phys. Chem.* **(2005)**, in preparation.
58. D. Grumelli, A. Wolosiuk, E. Forzani, G. A. Planes, C. Barbero, and E. J. Calvo, *Chem. Commun.* 3014 **(2003)**.

Received: XX XXXXX XXXX. Accepted: XX XXXXX XXXX.